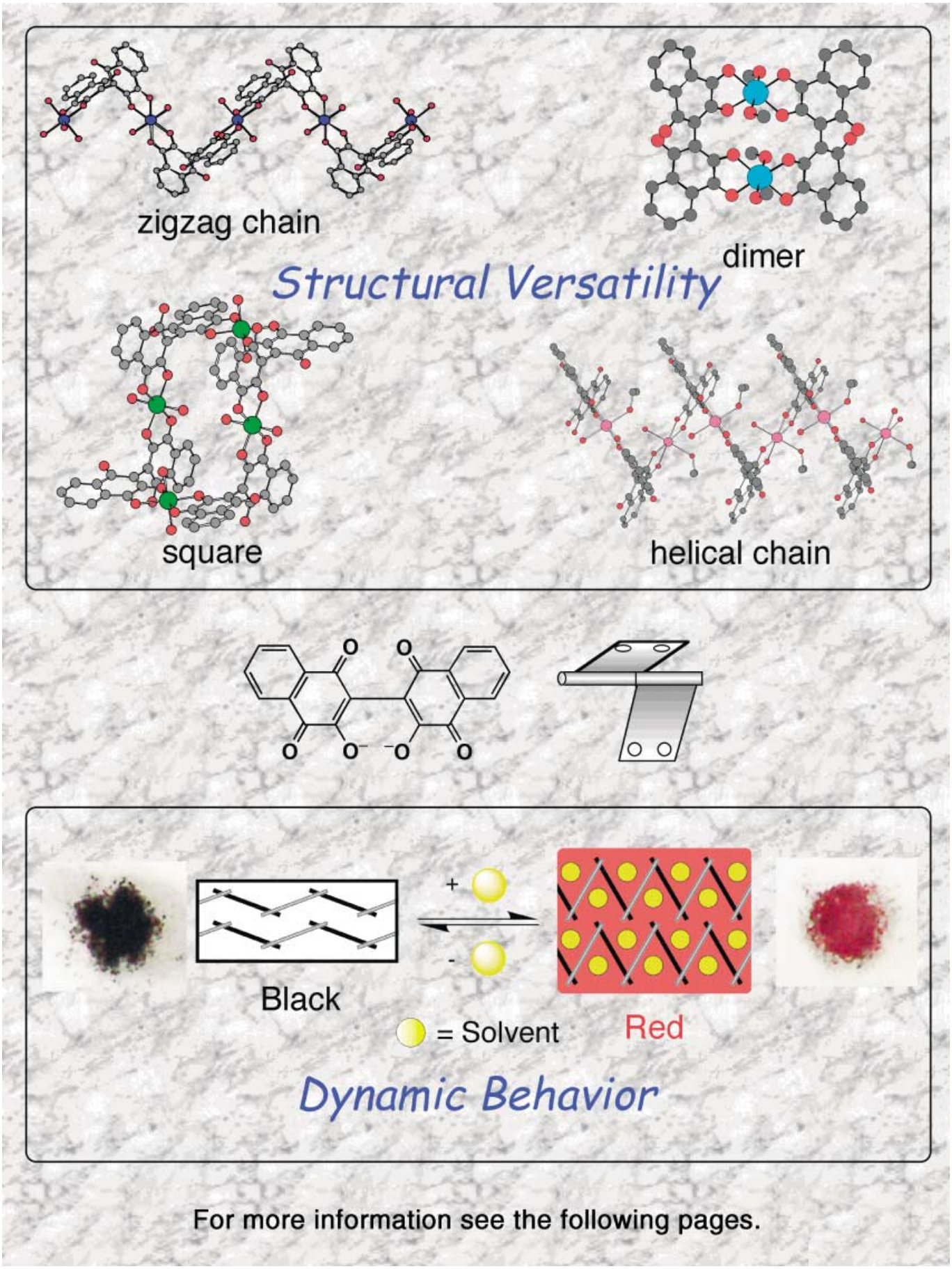

 DOI: 10.1002/chem.200305640

Metal-Complex Assemblies Constructed from the Flexible Hinge-Like Ligand H_2bhnq: Structural Versatility and Dynamic Behavior in the Solid State

Koichi Yamada,[a] Sadahiro Yagishita,[b] Hirokazu Tanaka,[b] Kazuhiro Tohyama,[b] Keiichi Adachi,[a] Sumio Kaizaki,[a] Hitoshi Kumagai,[c] Katsuya Inoue,[c] Ryo Kitaura,[d] Ho-Chol Chang,[d] Susumu Kitagawa,[d] and Satoshi Kawata*[a]

Abstract: Novel metal-complex assemblies constructed from the flexible hinge-like ligand H_2bhnq (H_2bhnq = 2,2′-bi(3-hydroxy-1,4-naphthoquinone)) have been synthesized. The X-ray crystal structures of these compounds reveal that four types of architectures are accessible by variation of the metal ions. In copper(II) compounds **1**–**3**, the chelating $bhnq^{2-}$ ions bridge copper(II) centers to form one-dimensional zigzag chains. The chains of **1**–**3** are arranged by hydrogen-bonding interactions and stacking interactions to produce porous structures. Cobalt(II) and zinc(II) compounds **4** and **5** form one-dimensional helical chains. In **4** and **5**, the crystal packing induces spontaneous resolution of the helical chains with chiral cavities formed perpendicular to the helices. Nickel(II) compounds **6** and **7** form cyclic tetramers. The fourth architecture, a dimer (compound **8**), is obtained by the reaction of zinc(II) and $bhnq^{2-}$ in MeOH. In these compounds, changes of the dihedral angles and the metal-coordination mode of the $bhnq^{2-}$ ion induce the structural versatility. The assemblies of the zigzag chains of the copper(II) compounds exhibit reversible vapochromic behavior. UV/Vis, powder X-ray diffraction, EPR, and adsorption isotherm measurements indicate that this vapochromic behavior is based on the hinge-like flexibility of the $bhnq^{2-}$ ion.

Keywords: coordination polymers · hydrogen bonds · self-assembly · vapochromism

Introduction

One of the goals of chemistry is the molecular design of materials to achieve specific or multifunctional properties.[1–5] Very successful approaches are molecular architecture and crystal engineering.[6–8] Within these two fields, a combination of metal ions with organic ligands was shown to be very fruitful in building multidimensional porous materials that possess high potential as absorbents for gas storage, molecular sieving, and catalysis.[9–11] The recent upsurge of reports on porous metal–organic frameworks has provided compelling evidence for the ability to design and produce structures with unusual pore shape, size, composition, and functionalities.[12–14] However, the rational design and preparation of metal–organic frameworks for specific applications are still at an early evolutionary stage; it is thought that the metal-organic frameworks should complement the inorganic ones since they exhibit properties such as enantioselectivity and conformational flexibility that are not displayed by zeolites. In particular, the flexibility of frameworks, which is expected to engender supramolecular isomerism or polymorphism[7,15] in the solid state, has until recently remained largely unexplored. Moreover, the use of metal-assembled

[a] Dr. K. Yamada, Dr. K. Adachi, Prof. S. Kaizaki, Prof. S. Kawata
Department of Chemistry, Graduate School of Science
Osaka University
Toyonaka, Osaka 560-0043 (Japan)
Fax: (+81) 6-6850-5408
E-mail: kawata@chem.sci.osaka-u.ac.jp

[b] S. Yagishita, H. Tanaka, K. Tohyama
Department of Chemistry, Shizuoka University
Ohya, Shizuoka, 422-8529 (Japan)

[c] Dr. H. Kumagai, Prof. K. Inoue
Institute for Molecular Science
Myoudaiji, Okazaki, Aichi 444-8585 (Japan)

[d] Dr. R. Kitaura, Dr. H.-C. Chang, Prof. S. Kitagawa
Department of Synthetic Chemistry and Biological Chemistry
Kyoto University
Saikyo-ku, Kyoto, 606-8501 (Japan)

Supporting information for this article is available on the WWW under http://www.chemeurj.org/ or from the author. Figure S1–S16, representing TG analysis data, powder XRD diagrams and ESR spectra of **1**, powder XRD diagrams, UV/Vis absorption spectra and ESR spectra of **2**, interchain hydrogen bonding interaction in **4**, ORTEP drawings of **8** and **9**, powder XRD diagrams of **4**, **5**, **7**–**10**.

DOI: 10.1002/chem.200305640

complexes with open framework structures has proved to be one of the best approaches to generate new materials with specificity for molecular recognition. Thus, the next step is to provide a dynamic metal-organic framework that responds to a specific guest molecule and changes its microcavities into cavities that are well-suited for the shape and/or affinity of the guest molecule.[16,17] On the other hand, macrocyclic tetranuclear complexes or molecular squares have been shown to behave as hosts for small guest molecules. Some have been shown to function as chemical sensors.[18,19] These compounds are often formed with rigid ligands, such as 4,4′-bipyridine, and with square-planar complexes employed as rigid metal corners. Such novel square architectures that consist of flexible ligands, which have conformational and geometrical freedom, provide further insight into supramolecular isomerism as well as the design of multifunctional materials. Therefore, much work is required to extend the knowledge of the relevant structural types and to establish rational synthetic strategies to the desired architectures using a flexible building module.

To construct novel nanosize architectures, we focused on the role of bridging ligands with conformational and geometrical flexibility. We chose 2,2′-bi(3-hydroxy-1,4-naphthoquinone) (H_2bhnq) as a bridging ligand (Scheme 1). This

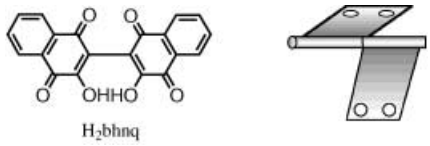

Scheme 1. Hinge-like ligand H_2bhnq.

ligand is a dimer of the natural product 3-hydroxy-1,4-naphthoquinone (lawsone[20]). The $bhnq^{2-}$ ion is capable, to a certain extent, of adjusting itself sterically owing to the flexible hinge-like ligand. There are two naphthoquinone groups in H_2bhnq and each group is linked by a single bond. The H_2bhnq has the virtue of allowing rotation about these single bonds. This rotation allows the conformational flexibility in H_2bhnq, that is, the ligand possesses skewed conformations. The degree of π conjugation in H_2bhnq is influenced by the dihedral angle between the naphthoquinone groups. As the metal ion can be employed as an angular directional unit, the incorporation of the hinge-like bridging ligands, which can change the degree of π conjugation, into a metal-complex assembly offers structural advantages for solid-state functional materials. First, there are at least four possible architectures of the assemblies that might reasonably exist: zigzag, helix, square, and dimer (Scheme 2). Metal-containing subunits with programmed dihedral angles can be employed for the self-assembly of frameworks, macromolecular polygons, and polyhedral cages. Moreover, the one-dimensional chain architectures are conformationally so flexible that the chains easily expand and contract with a change of the dihedral angles between naphthoquinone groups in the hinge-like ligands. Second, the hinge-like ligands enhance inter-ligand interactions using weak noncovalent interactions such as stacking and hydrogen-bonding in-

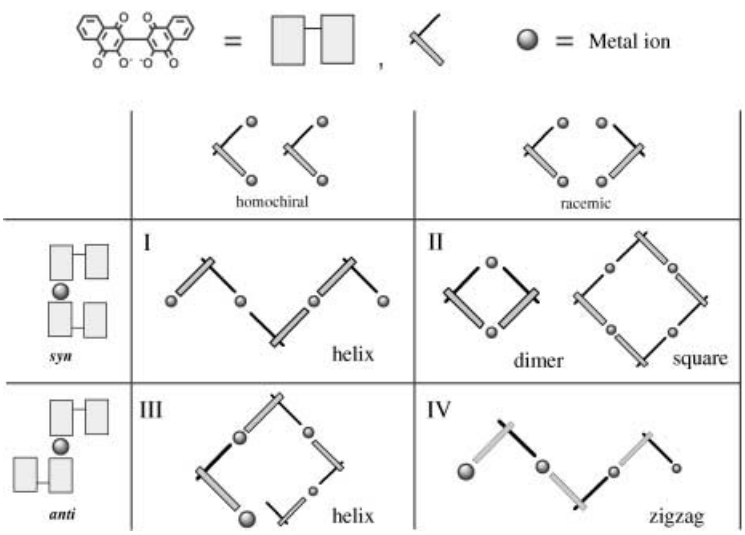

Scheme 2. Schematic representation of the assembled structures of the $bhnq^{2-}$ ion.

teractions, and thereby maintain the high stability of the solid-state structure.[21] Third, the cavities generated between adjacent complexes are sufficiently large to allow inclusion of guest molecules into the crystal. Fourth, the $bhnq^{2-}$ ion becomes chiral by virtue of the restricted rotation about the C–C bond linking the two lawsone units on ligation of the metal ions.

Taking advantages of these items, we demonstrate that 1) the assembly of the copper complex of $bhnq^{2-}$, the zigzag one-dimensional coordination polymer $\{[Cu(bhnq)(H_2O)_2](H_2O)(EtOH)_3\}_n$ (**1**), provides a material exhibiting vapochromic properties, 2) spontaneous resolution of the helical coordination polymers, $\{[Co(bhnq)(H_2O)(EtOH)](H_2O)_2(EtOH)\}_n$ (**4**) and $\{[Zn(bhnq)(H_2O)(THF)](H_2O)(THF)\}_n$ (**5**), reveal the existence of homochiral porous structures assembled from infinite helical chains. Moreover, we also describe 3) an advanced strategy to construct assemblies of molecular squares, and 4) the formation of the simplest architecture, a dimer.

Results and Discussion

Our synthetic strategy for constructing and operating the molecular hinge is schematically depicted in Scheme 2. There are four types of basic motifs that can be constructed from a [M(bhnq)] module connecting in a *trans* coordinating fashion, which causes the two $bhnq^{2-}$ anions to form a planar arrangement around the metal ion: type I: helical chain; type II: circle; type III: large rounded helix; type IV: zigzag chain. The modules can extend to form circles containing varying numbers of members by a change of the dihedral angle of the hinge (type II). Homochiral assemblies (type I and III) and racemic assemblies (type IV) can also be fabricated. The coordination geometry of $bhnq^{2-}$ (*syn* and *anti*; they are defined as a parallel or antiparallel arrangement of the two $bhnq^{2-}$ ions around the metal ion) also influences the shapes of the architectures. Therefore,

not only the dihedral angle, but also the metal connection mode and the coordination geometry of the molecular hinge are key tectonic factors for self-assembly. Moreover, the dynamic behavior of the molecular hinge and the assemblies induced by the change of the dihedral angle are controlled by hydrogen-bonding interactions. Herein we have structurally characterized the type IV zigzag chains for copper(II) complexes, type I helical chains for cobalt(II) and zinc(II) complexes, molecular squares which consist of type II + type III motifs for nickel(II) complexes, and a type II dimer for a zinc(II) complex with MeOH as solvent. The structures of these complexes are described below.

Crystal structure and vapochromic behavior of {[Cu(bhnq)-(H_2O)$_2$](H_2O)(EtOH)$_3$}$_n$ (1): The structure of **1** consists of a one-dimensional chain, [Cu(bhnq)(H_2O)$_2$]$_n$, and interstitial EtOH and water molecules. An ORTEP drawing of **1** is shown in Figure 1a. The chelating bhnq^{2-} ions bridge copper(II) centers in an "*anti*" fashion to form zigzag chains (type IV motif in Scheme 2), all of which extend parallel to the *c* axis (Figure 1b). There are two kinds of copper(II) units in the chain. The geometries around the metal ions are similar to each other, consisting of distorted octahedrons involving the four oxygen atoms of two bhnq^{2-} ions and two water molecules that are situated in *trans* positions to one another. The coordinated water molecules act as hydrogen-bond donors to interstitial water molecules and EtOH (vide infra).

The most interesting feature of the crystal structure is that the coordination polymer chains in **1** are arranged in such a way as to produce a rectangular structure with zigzag channels extended along the *c* axis (Figure 1c). The chains are each surrounded by four neighboring chains. This structure appears to be stabilized by two types of interactions;

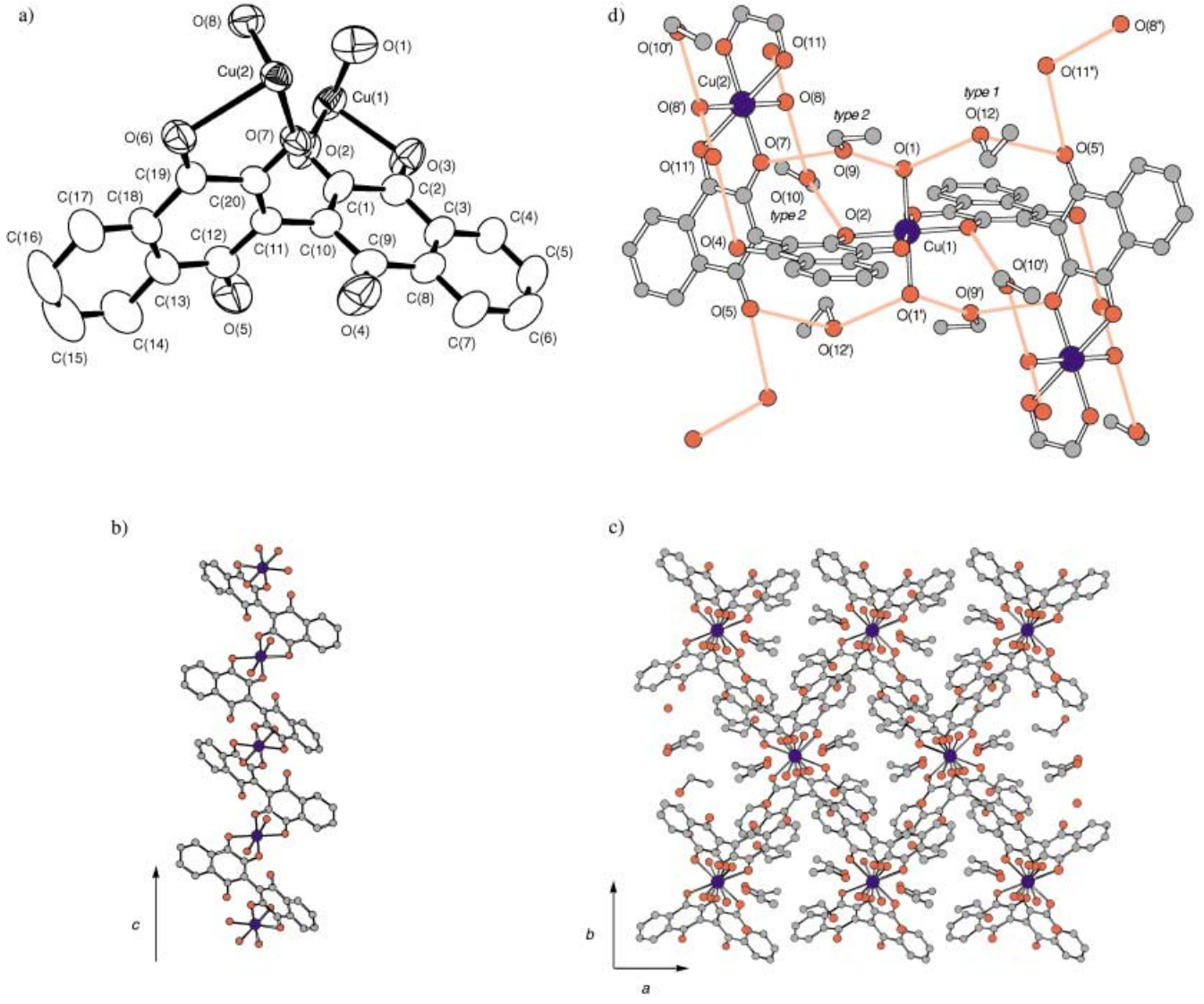

Figure 1. a) ORTEP drawing of an asymmetric unit of compound **1** with labeling scheme and thermal ellipsoids at the 50% probability level. Hydrogen atoms are omitted for clarity. Selected bond lengths [Å]: Cu(1)–O(1) 1.997(5), Cu(1)–O(2) 1.942(4), Cu(1)–O(3) 2.336(4), Cu(2)–O(6) 2.399(3), Cu(2)–O(7) 1.952(3), Cu(2)–O(8) 1.964(4). b) The Cu–bhnq chain of **1**. The dihedral angle of the bhnq^{2-} ions is 82.7° and the Cu···Cu distance bridged by a bhnq^{2-} ion is 6.57 Å. c) Assembled structure along the *c* axis. d) Hydrogen-bonding network of **1** between the chain and interstitial solvent molecules.

the efficient CH···O hydrogen-bonding interactions[21a] between the coordinated water oxygen O(8) and the carbon C(6′) atoms of the bridging $bhnq^{2-}$ ion on adjacent chains, and the stacking interactions between the $bhnq^{2-}$ ions on adjacent chains (C(5)–C(18′) 3.38 Å). The channels surrounded by the chains are filled with water and ethanol molecules (one water and three ethanol molecules per copper atom) that form a complicated hydrogen-bonded network (Figure 1d). There are two types of ethanol in the channel; type 1 is hydrogen-bonded to the coordinated water oxygen and the uncoordinated quinoid oxygen, and type 2 is hydrogen-bonded to the coordinated water oxygen and the coordinated quinoid oxygen atoms. Water molecules in the channel are hydrogen-bonded to the coordinated water oxygen and two uncoordinated quinoid oxygen atoms.

Interestingly, once removed from the mother liquor, the crystals quickly lose the interstitial ethanol, and the color of the crystals changes from red to black. The black sample, prepared from the red sample by drying under vacuum for two hours, has one interstitial water molecule in the channel (elemental analysis (%) calcd for $\{[Cu(bhnq)(H_2O)_2]\cdot(H_2O)\}_n$: C 52.0, H 3.06; found: C 51.2, H 3.16. thermogravimetric (TG) analysis data is shown in Figure S1 in the Supporting Information). This black powdered sample absorbs ethanol and quickly regains the original red color in an $EtOH/H_2O$ mixture. The reversibility is easily discernible using powder X-ray diffraction (see Figure S3 in the Supporting Information) and TG analysis (see Figure S2 in the Supporting Information). The original solvated crystal structure of **1** is regained, demonstrating the reversibility of the solvent-induced structural transition. The reversibility of the UV/Vis absorption behavior of compound **1** before and after being immersed was investigated to evaluate the absorption features responsible for the color changes (Figure 2). The shift in color is associated with the emergence of an ensemble of new absorption bands situated between 550 and 480 nm. The EPR spectrum of the red sample of **1** at 77 K has a signal with $g_{\parallel}=2.308$ and $g_{\perp}=2.068$, consistent with the elongated octahedral geometry, and a weak half-field transition band, indicative of the presence of the magnetic exchange interaction between the Cu^{2+} centers in the chain. While the EPR spectral line shape of the black sample is quite different from that of the red one, it also has a weak half-field transition band, indicating that the one-dimensional sequence of the complex is maintained under release of the solvent molecules (see Figure S4 in the Supporting Information). However, the intensity ratio between $\Delta M_s=1$ and 2 transitions of the red sample (2.2×10^{-4}) is bigger than that of the black one (1.1×10^{-4}), suggesting that the Cu–Cu distance in the chain of the red sample is shorter than that of the black one.[23]

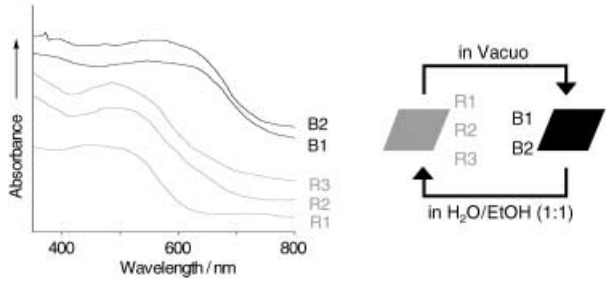

Figure 2. UV/Vis absorption spectra of **1** before and after being immersed.

To examine the porous properties, ethanol adsorption/desorption isotherms were measured for **1**. Figure 3 shows the isotherms in the pressure range P/P_0 0–1 at 298 K. Under these experimental conditions, the amount reabsorbed is about half of the original number of ethanol molecules per copper atom. The adsorption isotherm increases steeply with pressure in the first region ($P/P_0\approx0$–0.2), and it rises much more gradually in the second region ($P/P_0\approx0.2$–1.0). On the other hand, the desorption isotherm does not trace the adsorption isotherm, instead, it shows an abrupt drop ($P/P_0\approx0.18$–0.05). This hysteretic profile indicates the occurrence of a framework transformation in the crystal state, available for the guest inclusion.[17] Ethanol molecules can easily diffuse into the channels through hydrogen-bonding interactions between EtOH and $bhnq^{2-}$ ions; the attractive force would be strong enough to transform the channel structure so that the guest molecules are incorporated. The initial high uptake ($P/P_0\approx0$–0.2) indicates a strong sorbate–sorbant interaction, as evidenced by the shape of the isotherm in that pressure range. These results suggest that, upon incorporating guest molecules, the channels would undergo conformational changes, thus converting from an initial partially changed to a fully or near-fully changed entity, which exhibits sufficient lability towards binding incoming guest molecules.

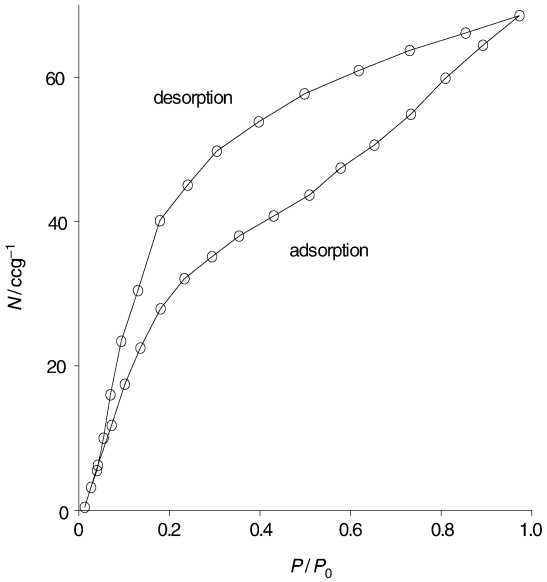

Figure 3. Ethanol adsorption and desorption isotherms at 298 K.

Based on the observed spectral and isothermal changes, a simple model is proposed to explain the vapochromic behavior[24] of **1**. The color change accompanying the loss of the solvent is consistent with the conformational change of the

$bhnq^{2-}$ ion. Indeed, the origin of the absorption band that appears is thought to be the transition of lawsone chromophores[25]. This spectral feature is influenced by the dihedral angle between the groups of the $bhnq^{2-}$ ion in the cases of $\{[Zn(bhnq)(H_2O)_2](H_2O)_2\}_n$ (**9**) and $\{[Zn(bhnq)(H_2O)(EtOH)](H_2O)(EtOH)_2\}_n$ (**10**) (116.3° (**9**) and 61.4° (**10**), Figure 4), which are black and red, respectively. These

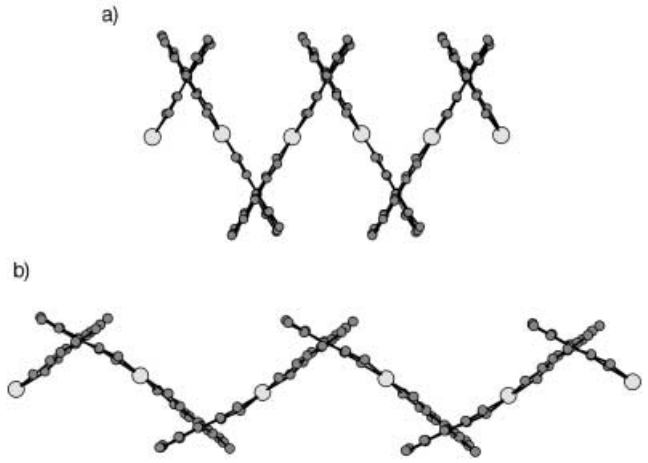

Figure 4. The Zn-bhnq chains of $\{[Zn(bhnq)(H_2O)(EtOH)](H_2O)(EtOH)_2\}_n$ (**10**) (a) and $\{[Zn(bhnq)(H_2O)_2](H_2O)_2\}_n$ (**9**) (b). The coordinated solvent molecules are omitted for clarity. The Zn···Zn distance bridged by a $bhnq^{2-}$ ion is 7.52 Å for **9** and 6.07 Å for **10**.

colors may be consistent with the π-electron delocalization due to the change of the dihedral angle of the $bhnq^{2-}$ ion. These structural differences are due to the hydrogen-bonding networks between the chain and the solvents. Thus, it is proposed that the ethanol molecules entering the channels of the black sample of **1** establish a hydrogen-bonding network with the $bhnq^{2-}$ ions and the coordinated waters, thereby contracting the chain and changing the dihedral angle of the $bhnq^{2-}$ ion (Scheme 3). On the other hand, the

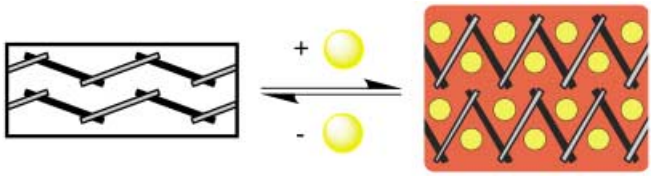

Scheme 3. Schematic representation of the vapochromic behavior.

black powdered sample also displays striking color changes upon exposure to certain alcoholic solvents in the vapor phase. For example, the solids immediately turn an intense vermilion color on exposure to methanol vapor, while alcoholic solvents that are larger than *n*-butyl alcohol are not absorbed due to size selectivity. All these color changes are reversible; the original black color is quickly regained under an ambient solvent-free atmosphere. However, the black powdered sample does not change to red by water vapor. This indicates that **1** has a high selectivity for a specific class of alcohols. Therefore, the occurrence of this reversible vapochromism demonstrates for the first time that the dynamic coil-like behavior of the one-dimensional chain, induced by the hinge-like properties of $bhnq^{2-}$, can be controlled through the change of the hydrogen-bonding interactions caused by the reversible and selective incorporation of alcoholic guest molecules.

The use of the $bhnq^{2-}$ ion for the synthesis of a novel coordination polymer that displays a large hysteretic isotherm, which is based on the response of the flexible and dynamic framework to specific guest molecules with color change, opens up further possibilities for the generation of third-generation porous materials.[16a]

Other copper compounds with different guests: The dynamic behavior of the vapochromism of **1** is based on the conformational flexibility of the molecular hinge. To investigate the influence of the solvent system on the formation of the supramolecular structure, the copper complexes $\{[Cu(bhnq)(THF)_2](THF)\}_n$ (**2**) and $\{[Cu(bhnq)(H_2O)_2](dioxane)(H_2O)_4\}_n$ (**3**) were synthesized. ORTEP drawings and assembled structures of **2** and **3** are shown in Figure 5. In both cases, the most interesting characteristics of the crystal structures are very similar to those of **1**, namely the 1D zigzag chains and the channel structures. However, the included solvent molecules and interactions between chains are different. The chelating $bhnq^{2-}$ ions bridge the copper(II) centers in an "*anti*" fashion to form zigzag chains (type IV motif in Scheme 2), all of which are extend parallel to the *c* axis. The geometries around the metal ions are distorted octahedrons, and involve the four oxygen atoms of two $bhnq^{2-}$ ions and two THF molecules for **2**, or two water molecules for **3**. The chain is surrounded by four neighboring chains and produces a rhombic structure with zigzag channels. In compound **2**, the assembled structure appears to be stabilized by two types of interactions; one is the efficient CH···O hydrogen-bonding interaction between the uncoordinated oxygen O(3) atom of the bridging $bhnq^{2-}$ ion and the C(5′) carbon atom of the bridging $bhnq^{2-}$ ion on the adjacent chains, and the other is the stacking interaction between the $bhnq^{2-}$ ions on the adjacent chains (for instance, the closest distance between the chains is approximately 3.6 Å (C(5)–C(9′)). On the other hand, in complex **3**, only stacking interactions exist between the $bhnq^{2-}$ ions on the adjacent chains (for instance, the closest distance between the chains is approximately 3.4 Å (C(2)–C(6′)). The channels surrounded by the chains are filled with guest molecules (one THF molecule for **2**, four water and one dioxane molecules for **3** per copper atom) that form a complicated hydrogen-bonded network. These results are consistent with our assumption that the network topologies are induced by guest molecules, owing to the flexibility of the ligand frameworks.

Similar to **1**, once removed from the mother liquor, compound **2** quickly loses the interstitial THF molecules and the color of the crystal changes from red to black. This dramatic color change is faster than **1**, and the original red color is regained on exposure to THF vapor. The reversibility is easily followed using powder X-ray diffraction. A portion of the

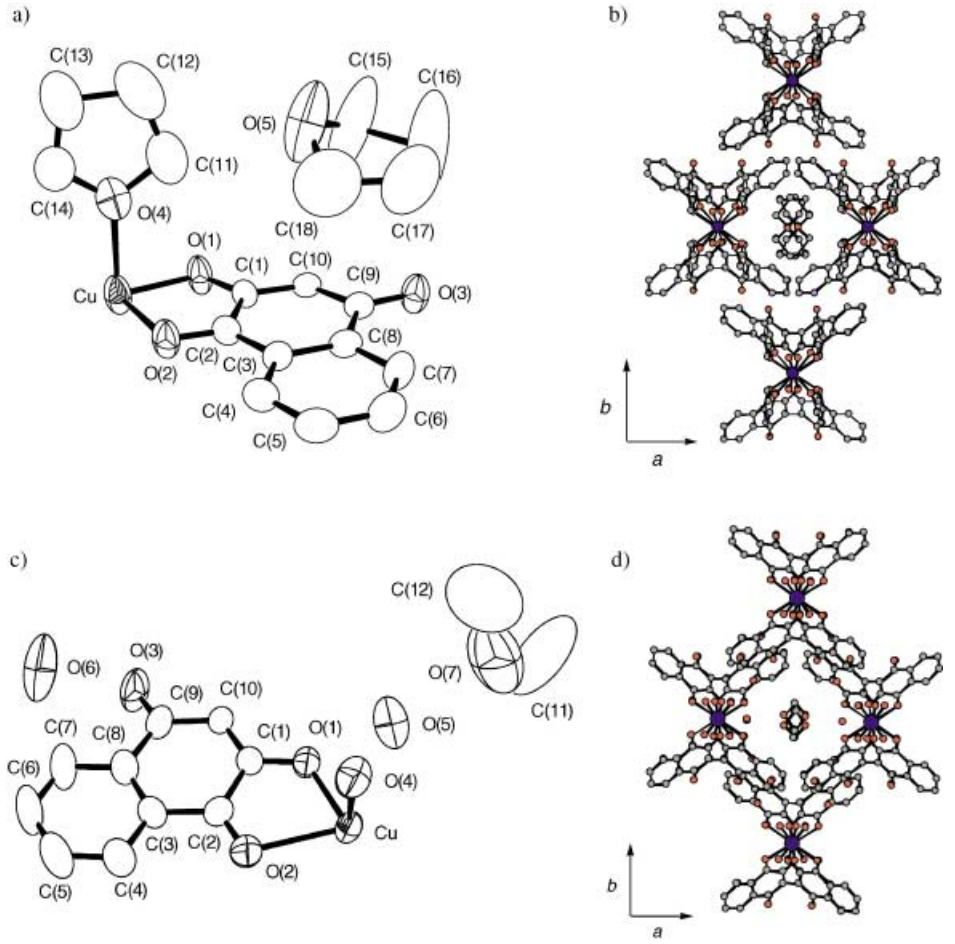

Figure 5. ORTEP drawings and assembled structures of compound **2** (a, b) and **3** (c, d). Selected bond lengths [Å]: Cu–O(1) 1.896(3), Cu–O(2) 2.051(3), Cu–O(4) 2.350(5) for **2**. Cu–O(1) 1.943(4), Cu–O(2) 2.360(4), Cu–O(4) 2.001(5) for **3**. The dihedral angle of the $bhnq^{2-}$ ions is 83.5° for **2**, 79.3° for **3**. The Cu···Cu distance bridged by a $bhnq^{2-}$ is 6.45 Å for **2**, 6.34 Å for **3**.

diffraction patterns of the original red sample, dried black sample and regained red sample are displayed in Figure S5. The original solvated crystal structure of $\{[Cu(bhnq)(thf_2)](THF)\}_n$ is regained, demonstrating the reversibility of the solvent-induced structural transition. The UV/Vis absorption spectra of the red and black samples were measured to evaluate the absorption feature responsible for the color change (see Figure S6 in the Supporting Information). The shift in color is associated with the emergence of an ensemble of new absorption bands around 500 nm. The EPR spectra of the powdered red and black samples of **2** at 77 K are shown in Figure S7 in the Supporting Information. The red sample displays a signal with $g \approx 2.2$, consistent with the elongated octahedral geometry, and the $\Delta M_s = 2$ transition around $g = 4$. The black sample, even though the line shape of EPR spectra is quite different from the red one, also shows the $\Delta M_s = 2$ transition, indicating that the one-dimensional sequence of the complex is maintained under release of the solvent molecules. The intensity ratio between the $\Delta M_s = 1$ and 2 transitions of the red sample (2.6×10^{-4}) is again bigger than that of the black sample (8.5×10^{-5}), suggesting that the Cu–Cu distance in the chain of the red sample is shorter than that of the black one. Thus, these features suggest that the reversible dramatic color change accompanying the loss of the solvent is fully consistent with the conformational change of the $bhnq^{2-}$ ion, that is, expansion of the chain. As a result, compound **2** expands/contracts the chain with the reversible desorption/absorption of solvent THF molecules accompanied by a change in color.

Helical structures of $\{[Co(bhnq)(H_2O)(EtOH)](H_2O)_2(EtOH)\}_n$ (4) and $\{[Zn(bhnq)(H_2O)(thf)](H_2O)(THF)\}_n$ (5) with chiral channels: The dynamic vapochromism behavior of **1** is based on the conformational flexibility of the molecular hinge. This can therefore be used for the introduction of not only alcohols, but also chiral molecules, since the model is inherently based on the flexibility and the hydrogen-bonding ability of the ligand. Thus, when H_2bhnq forms homochiral metal–organic porous materials that are assembled from chiral 1D chains, this may induce enantioselective properties in these materials.[26]

Compounds **4** and **5** crystallize as helical polymeric chains with large channels. The helices are generated around a crystallographic 2_1 axis. ORTEP drawings of **4** and **5** are shown in Figure 6 and 7, respectively. The chelating $bhnq^{2-}$ ions bridge the metal centers to form the helical chains in a "*syn*" fashion (type I motif in Scheme 2), all of which extend parallel to the *c* axis (Figure 6b and 7b). The geometries around the metal ions are distorted octahedrons that involve the four oxygen atoms of the two $bhnq^{2-}$ ions, and one water molecule, and one ethanol molecule for **4**, and one water molecule and one THF molecule for **5**. The coordinated water molecules act as hydrogen-bond donors to the interstitial solvent molecules.

Examination of the crystal packing in **4** and **5** reveals the existence of CH···O hydrogen-bonding interactions between the $bhnq^{2-}$ ligands on the adjacent helices in both compounds. In compound **4**, multiple hydrogen-bonding interactions[27] are operative between O(3)–C(16′), O(6)–C(15′), C(18)–O(5′), and C(17)–O(2″), which are, in turn, involved in an AADD-DDAA arrangement (A: hydrogen bond acceptor, D: hydrogen bond donor, see Figure S8 in the Supporting Information). On the other hand, there are two types of single hydrogen bonds in compound **5** (C(5)–O(6′)

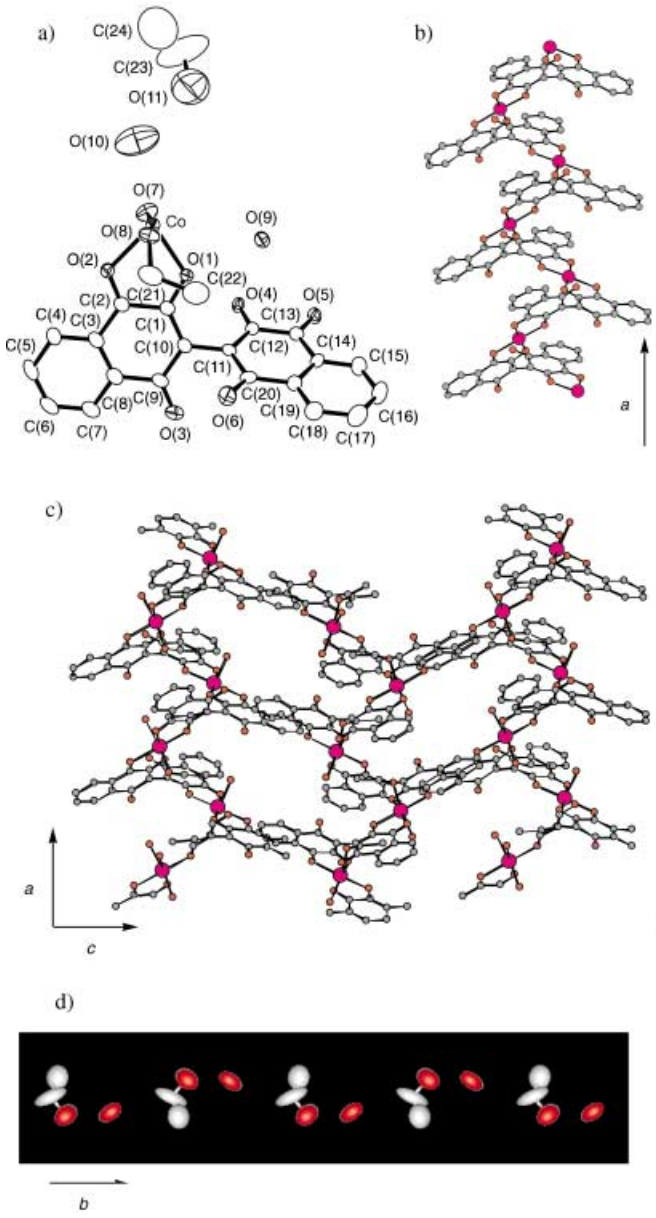

Figure 6. Crystal structure of **4**: a) ORTEP drawing of an asymmetric unit with labeling scheme and thermal ellipsoids at the 50% probability level. Selected bond lengths [Å]: Co–O(1) 2.035(2), Co–O(2) 2.141(3), Co–O(4) 2.038(2), Co–O(5) 2.134(3), Co–O(7) 2.058(3), Co–O(8) 2.086(3). b) The helical Co–bhnq chain. The dihedral angle of the $bhnq^{2-}$ ions is 61.4°. c) The homochiral porous structure along the *b* axis. d) The one-dimensional helical arrangement of the interstitial solvent molecules.

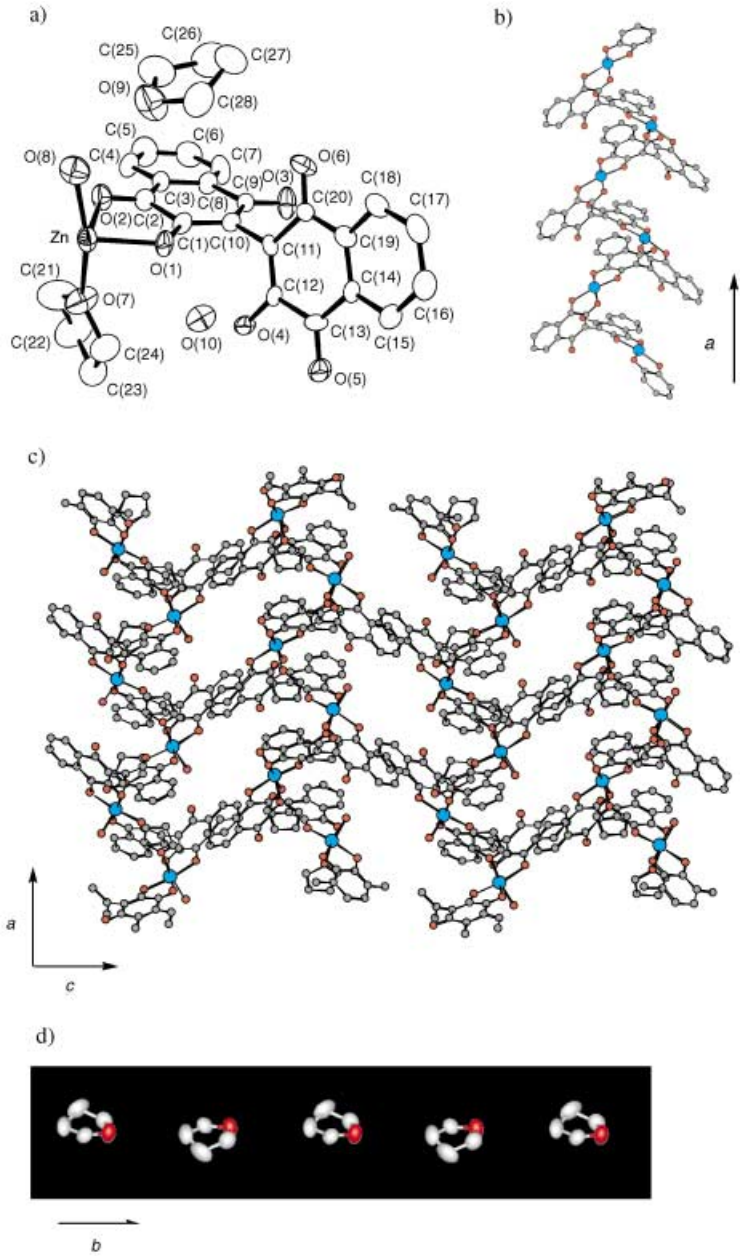

Figure 7. Crystal structure of **5**: a) ORTEP drawing of an asymmetric unit with labeling scheme and thermal ellipsoids at the 50% probability level. Selected bond lengths [Å]: Zn–O(1) 2.019(5), Zn–O(2) 2.135(5), Zn–O(4) 1.994(5), Zn–O(5) 2.184(5), Zn–O(7) 2.249(6), Zn–O(8) 2.038(8). b) The helical Zn–bhnq chain. The dihedral angle of the $bhnq^{2-}$ ions is 81.3°. c) The homochiral porous structure along the *b* axis. d) The one dimensional helical arrangement of the interstitial solvent molecules.

3.27 Å and C(16)–O(3′) 3.34 Å). The hydrogen bond is inherently directional and appears to manifest itself in two salient ways. First, the crystal packing induces spontaneous resolution of the helices, that is, homochiral helices align in each crystal. Second, adjacent helices are staggered by half the length of the unit cell in relation to one another. Consequently, the chiral cavities that are suitable for incorporation of the guest molecules exist perpendicular to the helices (Figure 6c, 7c). These channels contain an ordered helical arrangement[28] of solvent molecules generated around crystallographic 2_1 screw axes. The primary interaction between the solvent molecules and the walls of the cavities results from hydrogen bonds between the solvent molecules and coordinated water. A portion of one of the solvent chains is illustrated in Figure 6d and 7d and reveals that the helical chains are inherently polar. The chirality of the channels appears to induce chirality into the helical arrangements that are formed by the solvent molecules.

Nickel compounds: molecular squares with flexible corners: We designed the assembly of $bhnq^{2-}$ ions into square structures by linking them with transition-metal components

(Scheme 4). Two types of square architectures can be constructed from the basic motifs: boat (type II motif) and chair (type II + type III see Scheme 2). The $bhnq^{2-}$ ion can be employed as a "flexible ligand corner" for both square architectures. Molecular squares have often been formed

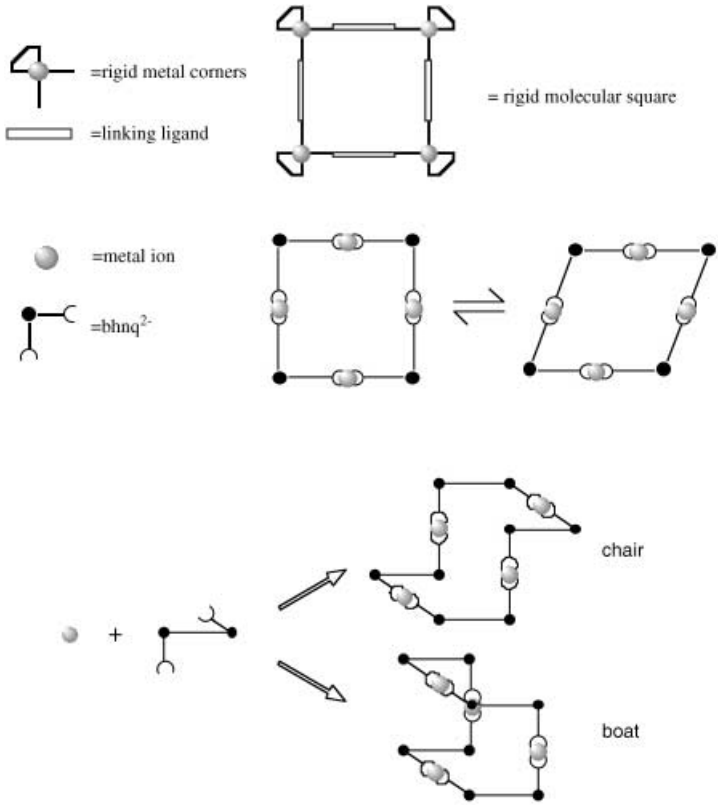

Scheme 4. Schematic representation of the molecular squares with the $bhnq^{2-}$ ion.

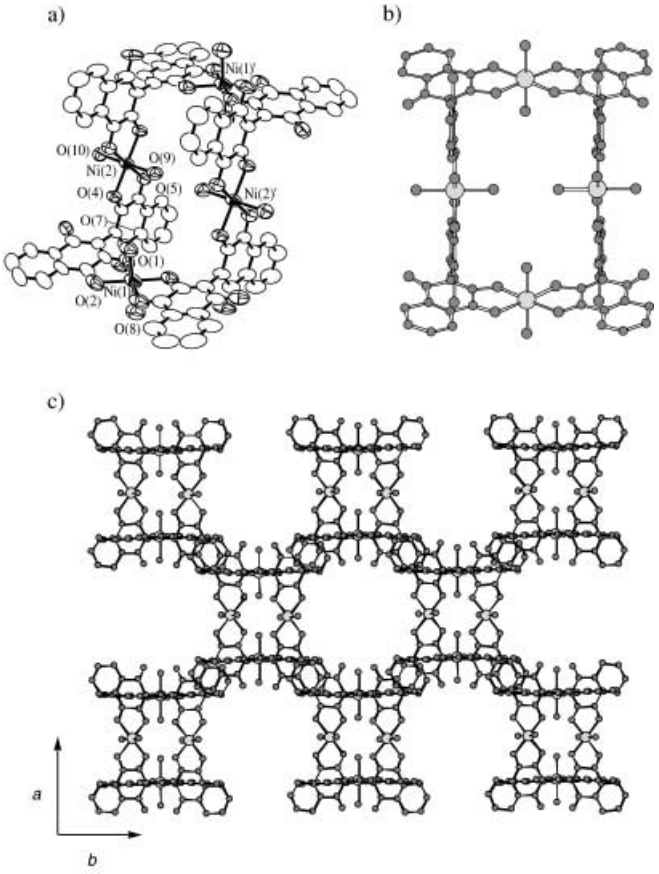

Figure 8. Molecular structure of the tetranuclear complex in the crystal of **6** emphasizing the chairlike structure (a) and the intramolecular cavity (b). Selected bond lengths [Å]: Ni(1)–O(1) 1.992(7), Ni(1)–O(2) 2.063(9), Ni(1)–O(7) 2.070(8), Ni(1)–O(8) 2.057(9), Ni(2)–O(4) 2.009(4), Ni(2)–O(5) 2.074(4), Ni(2)–O(9) 2.074(4), Ni(2)–O(10) 2.054(8). c) Checkered structure of **6** along the *c* axis. The interstitial solvent molecules are omitted for clarity.

with rigid ligands, such as 4,4′-bipyridine, and *cis*-Pd^{II} or *cis*-Pt^{II} square-planar complexes employed as "rigid metal corners".[18a,d] The corner angle of a square corresponds to the dihedral angle between two naphthoquinone groups of the $bhnq^{2-}$ diaion; the variation of the dihedral angle changes the molecular square from one conformation to the other. Therefore, the reversible conformational change of the architecture from a "rectangle" to a "rhombus" may be observed owing to the rotation around a single bond. Following the concept shown in Scheme 4, we synthesized such a flexible molecular square.

Two kinds of molecular square compounds were obtained by changing the solvent. $[Ni_4(bhnq)_4(H_2O)_8](H_2O)_{10}(EtOH)_6$ (**6**) is a cyclic self-assembled structure of four nickel(II) cations and four $bhnq^{2-}$ ions. The crystal structure of **6** is shown in Figure 8. The $bhnq^{2-}$ ion also acts as a 2-connecting ligand. There are two crystallographically distinct nickel(II) cations that have an octahedral environment, comprising two oxygen atoms from two water molecules and four oxygen atoms from two $bhnq^{2-}$ ions. The geometry around the Ni(1) atom, situated on a mirror plane, is a distorted octahedral arrangement with the four oxygen atoms of the two $bhnq^{2-}$ ions in a "*syn*" fashion. This feature is similar to those of the metal ions in the helical chains of **4** and **5**. On the other hand, a twofold symmetry axis perpendicular to the mirror plane passes through the Ni(2) atom. The coordination geometry of the Ni(2) atom resembles that of the Cu atom in compounds **1**–**3**; the $bhnq^{2-}$ ions coordinate to the nickel(II) center in a "*anti*" fashion. As a result, compound **6** forms the chairlike square architecture (type II + type III motif in Scheme 2), which has a larger intramolecular cavity (Ni–Ni separations within the cavity of approximately 7.5 × 12 Å; Figure 8b) which is occupied by four EtOH and two water molecules. Each tetranuclear complex stacks with the four adjacent tetranuclear complexes, and align to form a "checkered structure" (Figure 8c). The checkers further stack to form a three-dimensional structure with the channels, which are suitable for incorporation of the guest solvent molecules (Ni–Ni separations with the cavity of approximately 8 × 8 Å), perpendicular to the direction along which the checkers spread. These channels contain the interstitial water and EtOH molecules.

We have found another kind of structure (Figure 9) based on a cyclic tetranuclear complex $[Ni_4(bhnq)_4(H_2O)_8](H_2O)_{16}(THF)_4$ (**7**). The $bhnq^{2-}$ ion also acts as a 2-connecting ligand, binding to two nickel cations through two phen-

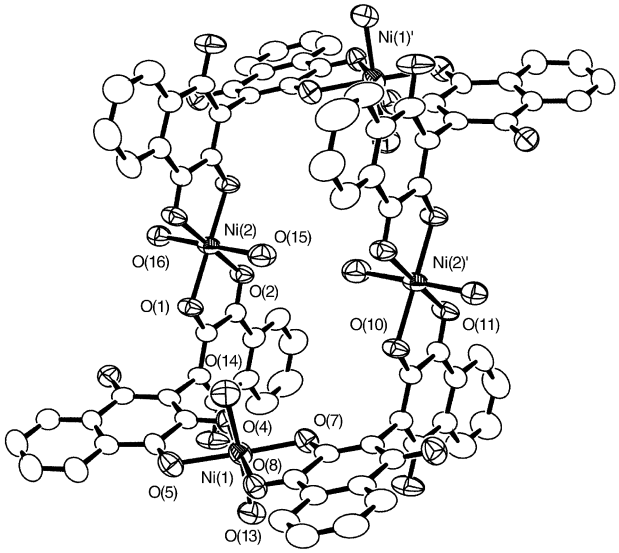

Figure 9. ORTEP drawing of the tetranuclear complex in the crystal of **7** with labeling scheme and thermal ellipsoids at the 50% probability level. Selected bond lengths [Å]: Ni(1)–O(4) 2.006(6), Ni(1)–O(5) 2.093(7), Ni(1)–O(7) 1.989(6), Ni(1)–O(8) 2.087(6), Ni(1)–O(13) 2.072(7), Ni(1)–O(14) 2.093(7), Ni(2)–O(1) 2.017(5), Ni(2)–O(2) 2.084(6), Ni(2)–O(10′) 2.014(5), Ni(2)–O(11′) 2.082(6), Ni(2)–O(15) 2.096(8), Ni(2)–O(16) 2.043(7).

oxy and two quinone carbonyl oxygen donors in **7**. Four donor sites on the $bhnq^{2-}$ ion are coordinated to the nickel(II) atom in a similar fashion to that observed in **6**. The coordination polyhedron is again octahedral, with Ni–O distances that do not differ significantly from those observed in **6**. There is a slight, but important, difference between the two compounds; the dihedral angle of the $bhnq^{2-}$ ion is 94.1° in **6**, while those of **7** are 96.5° and 102.4°, respectively. These features reveal that the conformational change shown in Scheme 4 is realized; compound **6** corresponds to a "rectangle", whereas **7** is a "rhombus", indicative of the remarkable solvent effect on the molecular structure. From the viewpoint of supramolecular chemistry, it is important to note that each dihedral angle of the four $bhnq^{2-}$ ions is not independent of the conformational change of one $bhnq^{2-}$ ion.

A dimeric structure of $[Zn_2(bhnq)_2(MeOH)_4](MeOH)_2$ (8): In the architectures shown in Scheme 2, the employed building block "[M(bhnq)]" is so flexible that we can construct three kinds of architectures; zigzag chain, helix and square. However, a dimer, which is the simplest architecture that can be constructed from the building block "[M(bhnq)]" using coordination-bonding interactions between the two connecting ligands and metal ions, has not yet being obtained under the above-described experimental conditions.

Fortunately we have succeeded, in spite of low yield, in growing red crystals of the dimeric compound by using methanol as solvent. An ORTEP drawing of **8** is shown in Figure 10a. The crystal structure indicates a type II motif consisting of two [Zn(bhnq)] modules, each of which is joined together to make a dimer. There is a crystallographic inversion center in the dimer, and the local chirality of the $bhnq^{2-}$ ions differs from one other. The geometry around

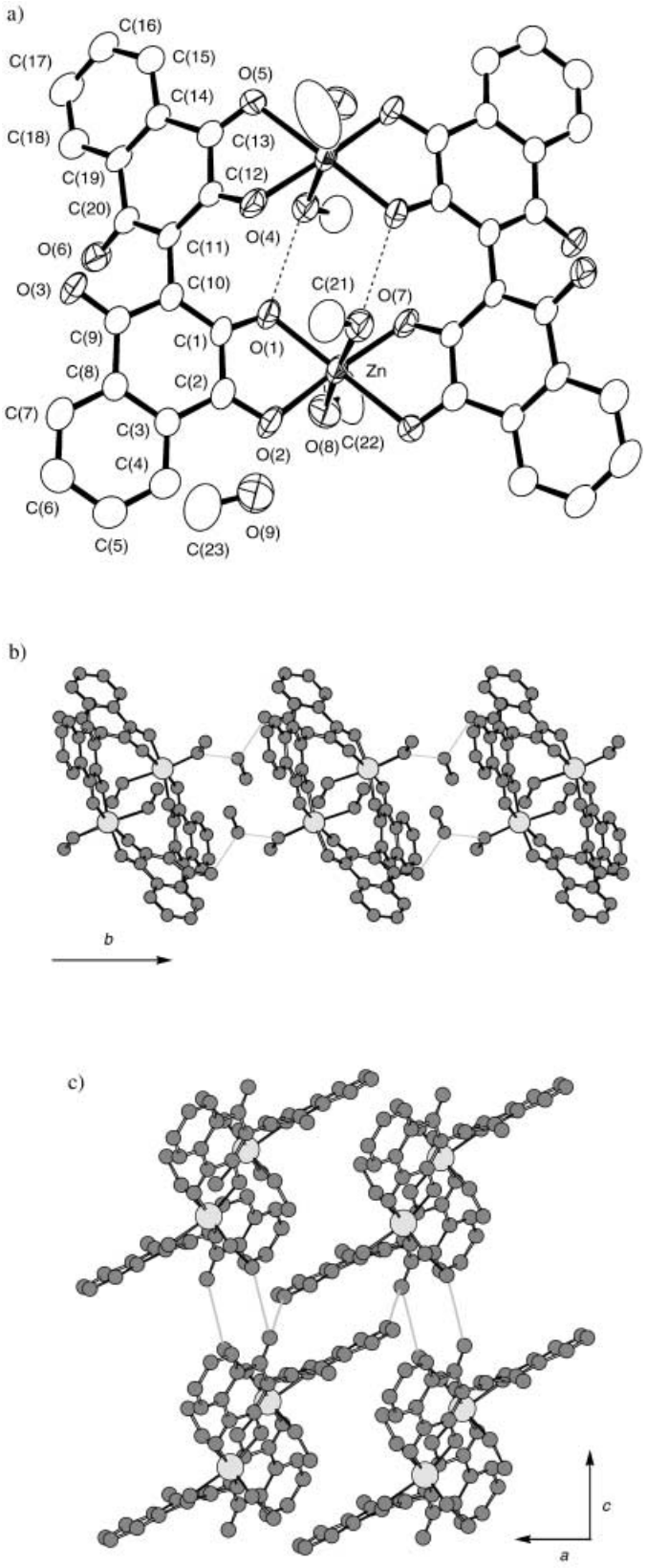

Figure 10. Crystal structure of **8**: a) ORTEP drawing with labeling scheme and thermal ellipsoids at the 50% probability level. Hydrogen atoms are omitted for clarity. Selected bond lengths [Å]: Zn–O(1) 2.026(5), Zn–O(2) 2.116(6), Zn–O(4) 1.993(5), Zn–O(5) 2.208(5), Zn–O(7) 2.291(6), Zn–O(8) 2.052(7). b) The hydrogen-bonded chain. c) Assembled structure along the *b* axis. The interstitial MeOH molecules omitted for clarity.

the zinc(II) ion is a distorted octahedral arrangement with the four oxygen atoms of the two $bhnq^{2-}$ ions arranged in a "*syn*" fashion, and two methanol molecules *trans* to one another. The dihedral angle of the $bhnq^{2-}$ ions is 50.4°, the smallest value for a dihedral angle found in the complexes obtained here. This is because the bridging sequence through the metal ions is restricted to a linear arrangement by the coordination properties of the metal ions, that is, due to the "rigid metal edges" that are always employed. Interestingly, there are three types of hydrogen bonds; one is an intra-dimer interaction, with hydrogen bonds to the coordinated methanol oxygen O(7) and the coordinated oxygen O(1′) atoms of the $bhnq^{2-}$ ion (2.80 Å). On the other hand, the other two types are inter-dimer interactions, with hydrogen bonds to interstitial methanol molecules linking the adjacent dimers (O(8)–O(9) 2.60, O(6)–O(9′) 2.72 Å) to form a one-dimensional chain (Figure 10b). Moreover, the hydrogen-bonded chains are associated through a complicated network: 1) two types of CH···O hydrogen-bonding interactions (O(3)–C(16′) 3.40, O(3)–C(22″) 3.28 Å), and 2) stacking interactions (nearest-neighbor C–C distance: 3.45 Å) (Figure 10c).

While the structures of dimeric **8** and helical **5** (and **9** and **10**) are constructed from the same building block "[Zn(bhnq)]", in compound **8** the difference of included solvents results in the different conformation (dihedral angle) for the $bhnq^{2-}$ ions, and therefore the different dimer structure. These differences may be brought about by the interactions between the included solvent molecules and the flexible metal–organic framework through hydrogen-bonding interactions. In compound **8**, the decreased hydrogen-bonding network with methanol prevents the elongation of the building block and the formation of the helical structure.

Conclusion

The present work demonstrates for the first time that a simple complex module can be pertinently assembled to produce various kinds of desired architectures by "a building-block methodology of the molecular hinge". The synthetic strategy proposed here for using a molecular hinge to construct flexible frameworks, to the best of our knowledge, is an important conceptual advance. The complex modules, $[M(bhnq)]_n$, are so flexible that they can vary the shape and the dimensionality of the assemblies by changes of the dihedral angles (50.4°–116.3°) and the metal-coordination mode (*syn* and *anti* fashion) of the $bhnq^{2-}$ ion. Consequently, the building blocks afford a surprising diversity of assembled structures (Scheme 5); 1) zigzag chains in **1**–**3** (type IV motif), 2) helical chains in **4** and **5** (and **9** and **10**) (type I motif), 3) molecular squares in **6** and **7** (type II + type III motif), and 4) a dimer in **8** (type II motif). Thus, the control of these features is one of the key factors to develop a pertinent synthesis strategy for the desired architectures from a simple building block with a molecular hinge. Interestingly, the selection of the metal mediates the tuning of the structures of the motifs and the conformation of the hinge; the trend of tuning by metal ions follows the ionic radii predicted by ligand field theory and the Jahn–Teller theorem.[29] Cobalt(II) and zinc(II) ions, which have the larger ionic radii (the average M–O distance: 2.08 Å for **4**, 2.10 Å for **5, 9**, and **10**), form helices while the nickel(II) ion, which has the smaller ionic radius (the average M–O distance: 2.05 Å for **6**, 2.06 Å for **7**), forms the square architecture. Only the copper(II) ion that is subject to Jahn–Teller distortion forms the zigzag motif. The structures of the motifs can therefore be described as the result of reading molecular information stored in the ligand by the metal ions. Furthermore, hydro-

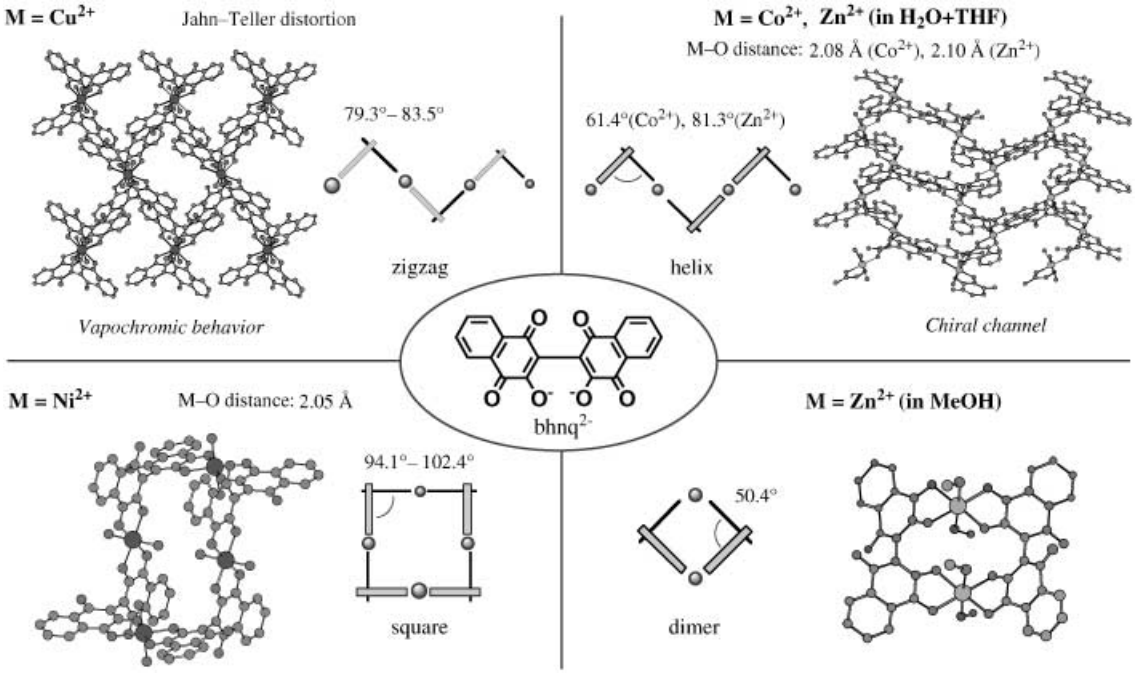

Scheme 5. Diversity of the assembled structures of the $bhnq^{2-}$ ion.

gen bonding increases the dimensionality of the system, and thus the selection of the solvent provides further structural varieties in the crystal structure.

The assembly of the zigzag chains of the copper compound **1** exhibits reversible vapochromic behavior. It provides a simple model which proposes that the vapochromic behavior is based on the hinge-like flexibility, that is, the coil-like behavior and the hydrogen-bonding properties of the ligand. In this system, the synthesis using the $bhnq^{2-}$ ion provides a novel coordination polymer, which exhibits a hysteretic isotherm based on the flexible and dynamic frameworks responding to specific guest molecules. This opens up a new field in porous coordination materials. Moreover, this stretching behavior of the chain with the molecular hinge will be applicable as nanoscale devices, "molecular muscles", and "molecular springs".[30] On the other hand, the helical chains of **4** and **5** are assembled to yield porous structures with chiral channels. The chirality of the channels appears to induce chirality into the helical arrangements of introduced solvents, which could contribute to the development of molecular-based recognition. The $bhnq^{2-}$ ion is also employed as the "flexible ligand corner" for the square architecture. The conformational flexibility of the bridging ligand, caused by the hinge-like property, permits the reversible conformational change of the architecture from a "rectangle" to a "rhombus". Moreover the smaller dihedral angle of the flexible ligand corner makes it possible to form the dimer architecture. These results have shown that it is possible to build novel architectures with unique functions by using hinge-like ligands.

Experimental Section

Materials: 2,2′-Bi(3-hydroxy-1,4-naphthoquinone)(H_2bhnq) was purchased from Aldrich Chemical Co. and used without further purification. All other materials were obtained from Wako Co. and used as received.

Syntheses

$\{[Cu(bhnq)(H_2O)_2](H_2O)(EtOH)_3\}_n$ (1): An aqueous solution of copper(II) sulfate pentahydrate (3 mL, 5 mmol L^{-1}) was transferred to a glass tube. An ethanolic solution of H_2bhnq (6 mL, 2.5 mmol L^{-1}) was poured into the tube without mixing the two solutions. Red plate crystals began to form within a week. One of these crystals was used for X-ray crystallography. Physical measurements were conducted on a polycrystalline powder that was synthesized as follows: A solution of H_2bhnq (1.0 mmol) in EtOH (400 mL) was added dropwise to copper(II) acetate anhydrate (1.0 mmol) dissolved in water (200 mL). Upon stirring of the mixture, a red powder appeared immediately. The compound was unstable in air due to the loss of some of the interstitial solvent molecules. Yield: about 35%.

$\{[Cu(bhnq)(THF)_2](THF)\}_n$ (2): An aqueous solution of copper(II) acetate anhydrate (3 mL, 2.5 mmol L^{-1}) was transferred to a glass tube. A THF solution (3 mL) of H_2bhnq (2.5 mmol L^{-1}) was poured into the tube without mixing the two solutions. Red plate crystals began to form within a week. One of these crystals was used for X-ray crystallography. Physical measurements were conducted on a polycrystalline powder that was synthesized as follows: A solution of H_2bhnq (2.5 mmol) in THF (100 mL) was added dropwise to copper(II) acetate anhydrate (2.5 mmol) dissolved in THF (100 mL). The compound was unstable in air due to the loss of some of the interstitial solvent molecules. Yield: about 40%.

$\{[Cu(bhnq)(H_2O)_2](dioxane)(H_2O)_4\}_n$ (3): An aqueous solution of copper(II) acetate anhydrate (3 mL, 2.5 mmol L^{-1}) was transferred to a glass tube. A dioxane solution (3 mL) of H_2bhnq (2.5 mmol·L^{-1}) was poured into the tube without mixing the two solutions. Red plate crystals began to form within a week. The compound was unstable in air due to the loss of some of the interstitial solvent molecules. Yield: about 80%.

$\{[Co(bhnq)(H_2O)(EtOH)](H_2O)_2(EtOH)\}_n$ (4): An aqueous solution of cobalt(II) acetate tetrahydrate (3 mL, 5 mmol L^{-1}) was transferred to a glass tube. An ethanolic solution (6 mL) of H_2bhnq (2.5 mmol L^{-1}) was poured into the tube without mixing the two solutions. Dark red pillar crystals began to form within a week. The compound was unstable in air due to the loss of some of the interstitial solvent molecules. Yield: about 25%.

$\{[Zn(bhnq)(H_2O)(thf)](H_2O)(THF)\}_n$ (5): An aqueous solution of zinc(II) acetate dihydrate (3 mL, 5 mmol L^{-1}) was transferred to a glass tube. A THF solution (6 mL) of H_2bhnq (2.5 mmol L^{-1}) was poured into the tube without mixing the two solutions. Red pillar crystals began to form within a week. The compound was unstable in air due to the loss of some of the interstitial solvent molecules. Yield: about 35%.

$[Ni_4(bhnq)_4(H_2O)_8](H_2O)_{10}(EtOH)_6$ (6): An aqueous solution of nickel (II) acetate tetrahydrate (3 mL, 5 mmol L^{-1}) was transferred to a glass tube. An ethanolic solution (6 mL) of H_2bhnq (2.5 mmol L^{-1}) was poured into the tube without mixing the two solutions. The solutions were allowed to stand at room temperature for a month and yielded a small amount of dark red crystals. The compound was unstable in air due to the loss of some of the interstitial solvent molecules. Yield: about 10%.

$[Ni_4(bhnq)_4(H_2O)_8](H_2O)_{16}(THF)_4$ (7): An aqueous solution of nickel (II) acetate tetrahydrate (5 mL, 5 mmol L^{-1}) was transferred to a glass tube. A THF solution (5 mL) of H_2bhnq (5 mmol L^{-1}) was poured into the tube without mixing the two solutions. The solutions were allowed to stand at room temperature for a month to give plate-shaped dark-red crystals. The compound was unstable in air due to the loss of some of the interstitial solvent molecules. Yield: about 30%.

$[Zn_2(bhnq)_2(MeOH)_4](MeOH)_2$ (8): A MeOH solution of zinc(II) acetate (3 mL, 5 mmol L^{-1}) was transferred to a glass tube. A MeOH solution (6 mL) of H_2bhnq (2.5 mmol L^{-1}) was poured into the tube without mixing the two solutions. A small amount of red plate crystals began to form within a month. The compound was unstable in air due to the loss of some of the interstitial solvent molecules. Yield: about 10%.

$\{[Zn(bhnq)(H_2O)_2](H_2O)_2\}_n$ (9): An aqueous solution of zinc(II) acetate (6 mL, 2.5 mmol L^{-1}) was transferred to a glass tube. A THF solution (3 mL) of H_2bhnq (5 mmol L^{-1}) was poured into the tube without mixing the two solutions. Black plate crystals began to form within a month. The compound was stable in air. Yield: 73%. Elemental analysis calcd (%): C 49.9, H 3.35; found: C 49.2, H 3.40.

$\{[Zn(bhnq)(H_2O)(EtOH)](H_2O)(EtOH)_2\}_n$ (10): A solution of zinc(II) acetate (4 mL, 2.5 mmol L^{-1}) in 1:1 (v/v) EtOH/H_2O was transferred to a glass tube. An ethanolic solution (4 mL) of H_2bhnq (2.5 mmol L^{-1}) was poured into the tube without mixing the two solutions. Red plate crystals began to form within a month. The compound was unstable in air due to the loss of some of the interstitial solvent molecules. Yield: about 60%.

Physical measurements: UV/Vis absorption spectra were measured on a Jasco V-570 spectrophotometer. EPR spectra were recorded at X-band frequency with a Bruker EMX 8/2.7 spectrometer operating at 9.5 GHz. X-ray powder diffraction data were collected on a Rigaku RINT 2000 diffractometer using $Cu_{K\alpha}$ radiation. Thermal gravimetric (TG) analyses were carried out with a Seiko Instruments SSC5200 Thermo-analyzer in a nitrogen atmosphere (heating rate: 10 K min^{-1}). The adsorption isotherms were measured using a Cahn R-100 electrobalance contained within a SUS steel pressure chamber, fitted with two separate lines for evacuation and adsorbate gas pressurization, respectively.

Crystallographic data collection and refinement of the structure: X-ray data collection was carried out using a Rigaku AFC7R diffractometer with graphite monochromated $Mo_{K\alpha}$ radiation for compound **1**. For **2**, all measurements were made on a Rigaku RAXIS-RAPID image-plate diffractometer with graphite-monochromated $Mo_{K\alpha}$ radiation. For **3**, all measurements were performed on a Rigaku AFC5R diffractometer with graphite-monochromated $Mo_{K\alpha}$ radiation. For **4** and **9**, all measurements were performed on a Rigaku Mercury charge-coupled device (CCD) system with graphite-monochromated $Mo_{K\alpha}$ radiation. For **5**, **6**, **7**, **8**, and **10**, all measurements were performed on a Macscience MXC3 diffractometer. Crystallographic data are given in Table 1. The structures were solved by standard direct methods and refined by using SHELXL-97.[22]

Table 1. Crystallographic data for **1**–**10**

Compound	**1**	**2**	**3**	**4**	**5**
formula	$Cu_1C_{26}O_{12}H_{32}$	$Cu_1C_{32}O_9H_{32}$	$Cu_1C_{24}O_{14}H_{28}$	$Co_1C_{24}O_{11}H_{26}$	$Zn_1C_{28}O_{10}H_{28}$
fw	600.08	624.15	604.02	549.40	589.89
crystal system	monoclinic	monoclinic	monoclinic	orthorhombic	orthorhombic
space group, Z	$P2_1/n$, 4	$C2/c$, 4	$C2/c$, 4	$P2_12_12_1$, 4	$P2_12_12_1$, 4
a [Å]	11.401(2)	11.163(4)	11.604(4)	7.946(3)	9.117(8)
b [Å]	18.465(3)	20.953(6)	18.511(3)	13.625(4)	12.672(3)
c [Å]	13.131(3)	12.898(3)	12.681(2)	22.132(6)	23.012(5)
α [°]					
β [°]	92.08(2)	105.73(2)	92.48(2)		
γ [°]					
V [Å^3]	2762.6(9)	2903.8(1)	2721.4(9)	2396.0(12)	2659(2)
ρ_{calcd} [g cm^{-3}]	1.443	1.428	1.474	1.523	1.474
diffractometer	AFC7R	RAXIS-RAPID	AFC5R	Mercury CCD	MXC3
radiation	$Mo_{K\alpha}$	$Mo_{K\alpha}$	$Mo_{K\alpha}$	$Mo_{K\alpha}$	$Mo_{K\alpha}$
temperature [K]	298	200	298	200	298
reflections collected	6638	9823	4272	25734	4045
independent reflections	6337	2803	3976	5475	3785
R_1, wR_2	0.057, 0.184	0.067, 0.158	0.069, 0.193	0.054, 0.125	0.062, 0.113
GOF	1.02	1.02	1.01	1.01	1.00
Compound	**6**	**7**	**8**	**9**	**10**
formula	$Ni_4C_{92}O_{48}H_{104}$	$Ni_4C_{96}O_{52}H_{112}$	$Zn_2C_{46}O_{18}H_{40}$	$Zn_1C_{20}O_{10}H_{16}$	$Zn_1C_{26}O_{11}H_{30}$
fw	2212.60	2332.71	1011.56	481.72	583.90
crystal system	monoclinic	triclinic	triclinic	monoclinic	monoclinic
space group, Z	$C2/m$, 2	$P\bar{1}$, 1	$P\bar{1}$, 1	$P2_1/c$, 4	$P2_1/n$, 4
a [Å]	18.576(2)	14.618(3)	8.6800(8)	8.136(1)	24.363(3)
b [Å]	21.508(3)	18.240(3)	11.227(1)	13.511(2)	8.022(1)
c [Å]	18.130(2)	14.088(4)	11.350(1)	16.703(3)	13.745(2)
α [°]		103.79(1)	85.631(8)		
β [°]	116.470(7)	99.44(1)	81.781(8)	90.941(9)	100.08(1)
γ [°]		109.81(1)	80.144(8)		
V [Å^3]	6484.2(13)	3306.6(1)	1077.0(2)	1835.8(5)	2644.8(7)
ρ_{calcd} [g cm^{-3}]	1.133	1.171	1.560	1.743	1.466
diffractometer	MXC3	MXC3	MXC3	Mercury CCD	MXC3
radiation	$Cu_{K\alpha}$	$Mo_{K\alpha}$	$Cu_{K\alpha}$	$Mo_{K\alpha}$	$Mo_{K\alpha}$
temperature [K]	298	298	298	200	298
reflections collected	4065	9193	3801	18096	7010
independent reflections	3815	9193	3412	4196	6075
R_1, wR_2	0.085, 0.253	0.120, 0.329	0.105, 0.318	0.052, 0.150	0.060, 0.147
GOF	1.01	1.15	1.31	1.09	0.99

Non-hydrogen atoms were found by successive full-matrix least-squares refinement on F^2 and refined with anisotropic thermal parameters. For all compounds, the positions of the interstitial solvent molecules were successfully determined, even though the thermal motions were relatively high for **6** and **7**. For **2** the interstitial THF molecule was disordered in two positions and for **6** one water and one EtOH molecule were disordered in one position with occupancies of 0.5. Hydrogen atoms of the $bhnq^{2-}$ ion were placed in idealized positions and fixed. All calculations were performed by using the CrystalStructure crystallographic software package of the Molecular Structure Corporation & Rigaku.

CCDC-222138 (**1**), CCDC-222132 (**2**), CCDC-222136 (**3**), CCDC-222139 (**4**), CCDC-222135 (**5**), CCDC-222137 (**6**), CCDC-222133 (**7**), CCDC-222130 (**8**), CCDC-222131 (**9**), and CCDC-222134 (**10**) contain the supplementary crystallographic data for this paper. These data can be obtained free of charge via www.ccdc.can.ac.uk/conts/retrieving.html (or from the Cambridge Crystallographic Centre, 12 Union Road, Cambridge CB21EZ, UK; fax: (+44) 1223-336033; or deposit@ccdc.cam.ac.uk).

Acknowledgments

This research was supported by a Grant-in-Aid for Scientific Research (No. 15550050), and by Grants-in-Aid for Scientific Research on Priority Areas (Nos. 413 and 417) from the Ministry of Education, Culture, Sports, Science, and Technology, Japan.

[1] J.-M. Lehn, *Supramolecular Chemistry*, VCH, Weinheim, **1995**.

[2] a) E. Coronado, J. R. Galán-Mascarós, C. J. Gómez-García, V. Laukhin, *Nature* **2000**, *408*, 447; b) B. Olenyuk, J. A. Whiteford, A. Fechtenkotter, P. J. Stang, *Nature* **1999**, *398*, 796; c) C. J. Kuehl, Y. K. Kryschenko, U. Radhakrishnan, S. R. Seidel, S. D. Huang, P. J. Stang, *Proc. Natl. Acad. Sci. USA* **2002**, *99*, 4932.

[3] a) H. Kishida, H. Matsuzaki, H. Okamoto, T. Manabe, M. Yamashita, Y. Taguchi, Y. Tokura, *Nature* **2000**, *405*, 929; b) T. Kato, *Science* **2002**, *295*, 2414; c) T. E. Mallouk, J. A. Gavin, *Acc. Chem. Res.* **1998**, *31*, 209; d) R. Lescouëzec, J. Vaissermann, C. Ruiz-Pérez, F. Lloret, R. Carrasco, M. Julve, M. Verdaguer, Y. Dromzee, D. Gattesch, W. Wernsdorfer, *Angew. Chem.* **2003**, *115*, 1521; *Angew. Chem. Int. Ed.* **2003**, *42*, 1483.

[4] a) K. Nagayoshi, M. K. Kabir, H. Tobita, K. Honda, M. Kawahara, M. Katada, K. Adachi, H. Nishikawa, I. Ikemoto, H. Kumagai, Y. Hosokoshi, K. Inoue, S. Kitagawa, S. Kawata, *J. Am. Chem. Soc.* **2003**, *125*, 221; b) S. Kitagawa, S. Kawata, *Coord. Chem. Rev.* **2002**, *224*, 11; c) S. Kawata, H. Kumagai, K. Adachi, S. Kitagawa, *J. Chem. Soc. Dalton Trans.* **2000**, 2409.

[5] a) S. Kawata, S. Kitagawa, M. Kondo, I. Furuchi, M. Munakata, *Angew. Chem.* **1994**, *106*, 1861; *Angew. Chem. Int. Ed. Engl.* **1994**, *33*, 1759; b) S. Kawata, S. Kitagawa, H. Kumagai, C. Kudo, H. Kamesaki, T. Ishiyama, R. Suzuki, M. Kondo, M. Katada, *Inorg. Chem.*

1996, *35*, 4449; c) S. Kawata, S. Kitagawa, H. Kumagai, T. Ishiyama, K. Honda, H. Tobita, K. Adachi, M. Katada, *Chem. Mater.* **1998**, *10*, 3902.

[6] a) C. B. Aakeröy, *Acta Crystallogr.* **1997**, *B53*, 569; b) C. B. Aakeröy, A. M. Beatty, B. A. Helfrich, *J. Am. Chem. Soc.* **2002**, *124*, 14425; c) D. Braga, F. Grepioni, *Acc. Chem. Res.* **2000**, *33*, 601; d) D. Braga, L. Maini, M. Polito, L. Scaccianoce, G. Cojazzi, F. Grepioni, *Coord. Chem. Rev.* **2001**, *216–217*, 225.

[7] a) B. Moulton, M. J. Zaworotko, *Chem. Rev.* **2001**, *101*, 1629; b) M. J. Zaworotko, *Chem. Commun* **2001**, *1*.

[8] a) S. R. Batten, R. Robson, *Angew. Chem.* **1998**, *110*, 1558; *Angew. Chem. Int. Ed.* **1998**, *37*, 1460; b) R. Robson, *J. Chem. Soc. Dalton Trans.* **2000**, 3735.

[9] a) M. Eddaoudi, D. B. Moler, H. Li, B. Chen, T. M. Reineke, M. O'Keeffe, O. M. Yaghi, *Acc. Chem. Res.* **2001**, *34*, 319; b) T. J. Barton, L. M. Bull, W. G. Klemperer, D. A. Loy, B. McEnaney, M. Misono, P. A. Monson, G. Pez, G. W. Scherer, J. C. Vartuli, O. M. Yaghi, *Chem. Mater.* **1999**, *11*, 2633; c) O. M. Yaghi, H. Li, C. Davis, D. Richardson, T. L. Groy, *Acc. Chem. Res.* **1998**, *31*, 474; d) H. Li, M. Eddaoudi, M. O'Keeffe, O. M. Yaghi, *Nature* **1999**, *402*, 276.

[10] a) M. Kondo, M. Shimamura, S. Noro, S. Minakoshi, A. Asami, K. Seki, S. Kitagawa, *Chem. Mater.* **2000**, *12*, 1288; b) S. Noro, S. Kitagawa, M. Kondo, K. Seki, *Angew. Chem.* **2000**, *112*, 2161; *Angew. Chem. Int. Ed.* **2000**, *39*, 2082; c) S. Takamizawa, W. Mori, M. Furihata, S. Takeda, K. Yamaguchi, *Inorg. Chim. Acta* **1998**, *283*, 268.

[11] a) A. Corma, *Chem. Rev.* **1997**, *97*, 2373; b) M. Fujita, K. Umemoto, M. Yoshizawa, N. Fujita, T. Kusukawa, K. Biradha, *Chem. Commun.* **2001**, 509; c) M. Fujita, Y. J. Kwon, S. Washizu, K. Ogura, *J. Am. Chem. Soc.* **1994**, *116*, 1151; d) M. P. Shores, L. G. Beauvais, J. R. Long, *J. Am. Chem. Soc.* **1999**, *121*, 775; e) D. V. Soldatov, J. A. Ripmeester, S. I. Shergina, I. E. Sokolov, A. S. Zanina, S. A. Gromilov, Y. A. Dyadin, *J. Am. Chem. Soc.* **1999**, *121*, 4179; f) H. J. Choi, T. S. Lee, M. P. Suh, *Angew. Chem.* **1999**, *111*, 1490; *Angew. Chem. Int. Ed.* **1999**, *38*, 1405.

[12] a) M. Eddaoudi, J. Kim, N. Rosi, D. Vodak, J. Wachter, M. O'Keeffe, O. M. Yaghi, *Science* **2002**, *295*, 469; b) B. Chen, M. Eddaoudi, S. T. Hyde, M. O'Keeffe, O. M. Yaghi, *Science* **2001**, *291*, 1021; c) M. Eddaoudi, J. Kim, J. B. Wachter, H. K. Chae, M. O′Keeffe, O. M. Yaghi, *J. Am. Chem. Soc.* **2001**, *123*, 4368.

[13] a) R. Kitaura, S. Kitagawa, Y. Kubota, T. C. Kobayashi, K. Kindo, Y. Mita, A. Matsuo, M. Kobayashi, H.-C. Chang, T. C. Ozawa, M. Suzuki, M. Sakata, M. Takata, *Science* **2002**, *298*, 2358; b) K. Seki, W. Mori, *J. Phys. Chem. B* **2002**, *106*, 1380; c) K. Biradha, M. Fujita, *J. Chem. Soc. Dalton Trans.* **2000**, 3805; d) K. Biradha, Y. Hongo, M. Fujita, *Angew. Chem.* **2000**, *112*, 4001; *Angew. Chem. Int. Ed.* **2000**, *39*, 3843; e) K. Kasai, M. Aoyagi, M. Fujita, *J. Am. Chem. Soc.* **2000**, *122*, 2140.

[14] a) K. S. Min, M. P. Suh, *J. Am. Chem. Soc.* **2000**, *122*, 6834; b) L. C. Tabares, J. A. R. Navarro, J. M. Salas, *J. Am. Chem. Soc.* **2001**, *123*, 383; c) A. J. Fletcher, E. J. Cussen, T. J. Prior, M. J. Rosseinsky, C. J. Kepert, K. M. Thomas, *J. Am. Chem. Soc.* **2001**, *123*, 10001; d) E. J. Cussen, J. B. Claridge, M. J. Rosseinsky, C. J. Kepert, *J. Am. Chem. Soc.* **2002**, *124*, 9574; e) G. J. Halder, C. J. Kepert, B. Moubaraki, K. S. Murray, J. D. Cashion, *Science* **2002**, *298*, 1762.

[15] J. Bernstein, R. J. Davey, J. O. Henck, *Angew. Chem.* **1999**, *111*, 3646; *Angew. Chem. Int. Ed.* **1999**, *38*, 3441.

[16] a) S. Kitagawa, M. Kondo, *Bull. Chem. Soc. Jpn.* **1998**, *71*, 1739; b) S. Noro, R. Kitaura, M. Kondo, S. Kitagawa, T. Ishii, H. Matsuzaka, M. Yamashita, *J. Am. Chem. Soc.* **2002**, *124*, 2568.

[17] a) R. Kitaura, K. Fujimoto, S. Noro, M. Kondo, S. Kitagawa, *Angew. Chem.* **2002**, *114*, 141; *Angew. Chem. Int. Ed.* **2002**, *41*, 133; b) R. Kitaura, K. Seki, G. Akiyama, S. Kitagawa, *Angew. Chem.* **2003**, *115*, 444; *Angew. Chem. Int. Ed.* **2003**, *42*, 428.

[18] a) M. Fujita, *Chem. Soc. Rev.* **1998**, *27*, 417; b) R. V. Slone, K. D. Benkstein, S. Belanger, J. T. Hupp, I. A. Guzei, A. L. Rheingold, *Coord. Chem. Rev.* **1998**, *171*, 221; c) P. H. Dinolfo, J. T. Hupp, *Chem. Mater.* **2001**, *13*, 3113; d) S. Leininger, B. Olenyuk, P. J. Stang, *Chem. Rev.* **2000**, *100*, 853; e) F. A. Cotton, C. Lin, C. A. Murillo, *Acc. Chem. Res.* **2001**, *34*, 759.

[19] a) Y. Zhang, S. Wang, G. D. Enright, S. R. Breeze, *J. Am. Chem. Soc.* **1998**, *120*, 9398; b) S. J. Lee, W. Lin, *J. Am. Chem. Soc.* **2002**, *124*, 4554; c) R. Ziessel, L. Charbonniere, M. Cesario, T. Prange, H. Nierengarten, *Angew. Chem.* **2002**, *114*, 1017; *Angew. Chem. Int. Ed.* **2002**, *41*, 975; d) S. Toyota, C. R. Woods, M. Benaglia, R. Haldimann, K. Warnmark, K. Hardcastle, J. S. Siegel, *Angew. Chem.* **2001**, *113*, 773; *Angew. Chem. Int. Ed.* **2001**, *40*, 751.

[20] P. Garge, R. Chikate, S. Padhye, J. M. Savariault, P. De Loth, J. P. Tuchagues, *Inorg. Chem.* **1990**, *29*, 3315.

[21] a) G. R. Desiraju, T. R. Steiner, *The Weak Hydrogen Bond in Structural Chemistry and Biology*, Oxford University Press, Oxford, **1999**; b) G. R. Desiraju, *J. Chem. Soc. Dalton Trans.* **2000**, 3745; c) T. Steiner, *Angew. Chem.* **2002**, *114*, 50; *Angew. Chem. Int. Ed.* **2002**, *41*, 48; d) E. A. Meyer, R. K. Castellano, F. Diederich, *Angew. Chem.* **2003**, *115*, 1244; *Angew. Chem. Int. Ed.* **2003**, *42*, 1210.

[22] G. M. Sheldrick, SHELXL97, University of Göttingen, Germany, **1997**.

[23] A. Bencini, D. Gatteschi, *EPR of Exchange Coupled Systems*, Springer, Berlin, **1990**.

[24] a) C. E. Buss, K. R. Mann, *J. Am. Chem. Soc.* **2002**, *124*, 1031; b) C. E. Buss, C. E. Anderson, M. K. Pomije, C. M. Lutz, D. Britton, K. R. Mann, *J. Am. Chem. Soc.* **1998**, *120*, 7783; c) L. G. Beauvais, M. P. Shores, J. R. Long, *J. Am. Chem. Soc.* **2000**, *122*, 2763; d) N. A. Rakow, K. S. Suslick, *Nature* **2000**, *406*, 710; e) M. Albrecht, M. Lutz, A. L. Spek, G. V. Koten, *Nature* **2000**, *406*, 970.

[25] a) M. C. Rath, H. Pal, T. Mukherjee, *J. Chem. Soc. Faraday Trans.* **1996**, *92*, 1891; b) M. E. Bodini, P. E. Bravo, V. Arancibia, *Polyhedron* **1994**, *13*, 497.

[26] a) T. J. Prior, M. J. Rosseinsky, *Inorg. Chem.* **2003**, *42*, 1564; b) C. J. Kepert, T. J. Prior, M. J. Rosseinsky, *J. Am. Chem. Soc.* **2000**, *122*, 5158; c) J. S. Seo, D. Whang, H. Lee, S. I. Jun, J. Oh, Y. J. Jeon, K. Kim, *Nature* **2000**, *404*, 982.

[27] a) D. C. Sherrington, K. A. Taskinen, *Chem. Soc. Rev.* **2001**, *30*, 83; b) Y. Sugiyama, K. Adachi, S. Kawata, H. Kumagai, K. Inoue, M. Katada, S. Kitagawa, *CrystEngComm* **2000**, *2*, 174; c) X. Xu, S. L. James, D. M. P. Mingos, A. J. P. White, D. J. Williams, *J. Chem. Soc. Dalton Trans.* **2000**, 3783.

[28] a) K. Adachi, H. Irikawa, K. Shiratori, Y. Sugiyama, S. Kawata, *CrystEngComm* **2001**, *3*, 128; b) H. Gudbjartson, K. Biradha, K. M. Poirier, M. J. Zaworotko, *J. Am. Chem. Soc.* **1999**, *121*, 2599; c) K. Biradha, C. Seward, M. J. Zaworotko, *Angew. Chem.* **1999**, *111*, 584; *Angew. Chem. Int. Ed.* **1999**, *38*, 492.

[29] F. A. Cotton, L. M. Daniels, C. A. Murillo, J. F. Quesada, *Inorg. Chem.* **1993**, *32*, 4861.

[30] a) J.-P. Collin, C. Dietrich-Buchecker, P. Gaviña, M. C. Jimenez-Molero, J.-P. Sauvage, *Acc. Chem. Res.* **2001**, *34*, 477; b) M. J. Marsella, *Acc. Chem. Res.* **2002**, *35*, 944; c) O.-S. Jung, Y. J. Kim, Y.-A. Lee, J. K. Park, H. K. Chae, *J. Am. Chem. Soc.* **2000**, *122*, 9921; d) K. Tanaka, H. Osuga, Y. Kitahara, *J. Org. Chem.* **2002**, *67*, 1795.

Received: October 20, 2003

Published online: April 23, 2004